ELSEVIER

Computers & Geosciences 32 (2006) 1600–1614

COMPUTERS & GEOSCIENCES

www.elsevier.com/locate/cageo

Coupled model of surface water flow, sediment transport and morphological evolution

Guy Simpson[a,*], Sébastien Castelltort[b,1]

[a]Department of Earth Science, ETH Zurich, 8092 Zurich, Switzerland
[b]Institut für Geologie, Haldenbachstr. 44, HAD F1, ETH Zentrum, CH-8092 Zürich, Switzerland

Received 13 July 2005; received in revised form 21 February 2006; accepted 23 February 2006

Abstract

This paper presents a mathematical model coupling water flow and sediment transport dynamics that enables calculating the changing surface morphology through time and space. The model is based on the shallow water equations for flow, conservation of sediment concentration, and empirical functions for bed friction, substrate erosion and deposition. The sediment transport model is a non-capacity formulation whereby erosion and deposition are treated independently and influence the sediment flux by exchanging mass across the bottom boundary of the flow. The resulting hyperbolic system is solved using a finite volume, Godunov-type method with a first-order approximate Riemann solver. The model can be applied both to short time scales, where the flow, sediment transport and morphological evolution are strongly coupled and the rate of bed evolution is comparable to the rate of flow evolution, or to relatively long time scales, where the time scale of bed evolution associated with erosion and/or deposition is slow relative to the response of the flow to the changing surface and, therefore, the classical quasi-steady approximation can be invoked. The model is verified by comparing computed results with documented solutions. The developed model can be used to investigate a variety of problems involving coupled flow and sediment transport including channel initiation and drainage basin evolution associated with overland flow and morphological changes induced by extreme events such as tsunami.

Keywords: Shallow water equations; Erosion; Deposition; Channel spacing; Riemann solver; Finite volume method; Numerical modelling

1. Introduction

One of the main factors responsible for erosion and deposition at the Earth's surface is sediment transport in flowing water. Water flow induces sediment transport and changes in the surface morphology, which in turn modify the flow. This process involves two sets of dynamics which are intimately coupled, one related to the flowing fluid which is rapid, and the other related to entrainment and deposition which is usually relatively slow. Typically, studies focussing on short time scales and small spatial scales tend to focus on flow dynamics (e.g., engineers studying dam-break hydraulics or flood risk caused by extreme rainfall events), whereas scientists interested in long time scales

*Corresponding author.
E-mail addresses: simpson@erdw.ethz.ch (G. Simpson), sebastien.castelltort@lgs.jussieu.fr (S. Castelltort).
[1]Now at Laboratoire de Tectonique Université Pierre et Marie Curie, UMR 7072 4, place Jussieu T.46-45, E2 75252 Paris Cedex.

0098-3004/$ - see front matter © 2006 Elsevier Ltd. All rights reserved.
doi:10.1016/j.cageo.2006.02.020

and relatively large length scales focus more on the substrate erosion and/or deposition dynamics. Having said that, engineers are now beginning to recognize the practical importance of a mobile bed in influencing flow dynamics (e.g., Cao et al., 2004), while research scientists are recognizing the importance of flow dynamics in explaining landscapes (e.g., Roth et al., 1989; Izumi and Parker, 1995, 2000) and sedimentary deposits (e.g., Allen and Hoffman, 2005). A major challenge at present, and in the future, is to understand how flow and transport dynamics interact and how this coupling is manifest in landscapes and sedimentary deposits.

The purpose of this paper is to present a mathematical model which couples water flow and sediment transport dynamics that enables calculating the changing surface morphology through time and space (in two horizontal dimensions). The development of this model was motivated by the following three main factors. First, many scientific problems cannot be solved by neglecting flow dynamics (i.e., assuming that water moves as a gravity-driven flow in which dissipative forces associated with frictional resistance are balanced by the tendency for downslope movement, called the 'normal flow' model), something done in many current surface process models. For example, Smith and Bretherton (1972) demonstrated, using a linear stability analysis, the failure of the normal flow model in selecting a finite channel spacing when studying controls on channel initiation (see also Loewenherz, 1994, 1991). Izumi and Parker (1995, 2000) have since shown, also with a linear stability analysis, that the channel spacing problem is resolved by studying the full equations for shallow overland flow. These authors concluded stating that 'the flow model...is probably a better place to start in constructing a full model of drainage basin evolution than the normal flow model' (Izumi and Parker, 1995). The present study appears to be one of the first to attempt this in two spatial dimensions. Second, surface process models based on empirical drainage area–discharge relationships require a suite of additional equations between properties such as channel width, channel slope, water depth, hydraulic radius, and mean flow velocity (e.g., see Tucker and Slingerland, 1997). Although some of these equations have a good theoretical basis, many are solely empirical and most apply, only strictly, to alluvial rivers (also see discussion by Stark and Stark, 2001). Most of these problematic relationships can be by-passed by solving directly for flow velocities and water depth from the flow equations as is done here. Third, many models coupling sediment transport and water flow apply only to either supply-limited (e.g., Howard, 1994) or transport-limited (e.g., Simpson and Schlunegger, 2003) conditions. Some models based on the concept of sediment transport capacity include both classes as end-member cases (e.g., Kooi and Beaumont, 1994), although these models suffer from the problem that little is known about the time scale of entrainment mechanisms relative to that of the sediment transport required to achieve capacity. An alternative attractive approach is the so-called 'non-capacity' formulation (Cao et al., 2004, see also Crave and Davy, 2001). The difference between this approach compared to capacity formulations is that, rather than computing erosion or deposition based on whether the transport capacity is greater or less than the actual sediment discharge, erosion and deposition are treated as independent empirical functions and influence the sediment flux by exchanging mass across the bottom boundary of the flow.

The model presented in this study includes the shallow water equations for flow, conservation of sediment concentration, and empirical functions for bed friction, substrate erosion and deposition. Similar coupled sediment transport surface water flow models have been developed recently by Fagherazzi and Sun (2003) and Cao et al. (2004). The model here differs from these in that (1) it is two-dimensional and (2) it can be applied both to short time scales where the flow, sediment transport and morphological evolution are strongly coupled and the rate of bed evolution is comparable to the rate of flow evolution (e.g., erosion and deposition related to a dam break or tsunami), or to relatively long time scales where the time scale of bed evolution associated with erosion and/or deposition is slow relative to the response of the flow to the changing surface and therefore the classical quasi-steady approximation can be invoked (e.g., erosion due to overland flow driven by steady rainfall). The governing equations form a hyperbolic system which is solved numerically using a finite volume, Godunov-type method with a first-order approximate Riemann solver (Toro, 2001). While more accurate techniques are available to solve these equations this scheme is utilized for its simplicity, efficiency and robustness. The intention of this work is to describe in detail how this numerical method can be implemented to solve a system of equations which have a wide range of applicability in Earth

Science. The model presented is not intended to replace existing models which couple water flow and sediment transport, but rather it provides a means of addressing problems where flow dynamics are important, that more simplified models, based on normal-flow, cannot investigate. Having said that, we do feel that there is a need to rethink the governing equations used in many current models and that the formulation presented may offer new insight, not only concerning physical problems, but also regarding how one goes about modelling these problems. It is our view that this approach is likely to become more common in the future as earth scientists increasingly appreciate the importance of highly transient, extreme events, in forming landscapes and sedimentary deposits.

The remainder of the paper is organized as follows. First, the governing equations are presented. Second, the numerical method used to solve the equations is outlined in detail. Third, the accuracy of the model is tested against published solutions in the literature. Fourth, several potential applications of the model are briefly demonstrated. Finally, some conclusions are drawn and some comments on future work are made.

2. Governing equations

The formulation presented is based on shallow water theory, which assumes that the vertical component of acceleration has a negligible effect on the fluid pressure (i.e., pressure is hydrostatic). The resulting shallow water equations, which are obtained by depth-averaging the Navier–Stokes equations, are widely used to model free surface water flows over land or in open channels. For the case of flow over a mobile bed, the shallow water equations are coupled to equations for the conservation of sediment mass and evolution of bed topography. In two space dimensions, the complete system of equations are

$$\frac{\partial h}{\partial t}+\frac{\partial (hu)}{\partial x}+\frac{\partial (hv)}{\partial y}=\alpha+\frac{E-D}{1-\phi}, \tag{1}$$

$$\frac{\partial (hu)}{\partial t}+\frac{\partial}{\partial x}\left(hu^2+\frac{1}{2}gh^2\right)+\frac{\partial}{\partial y}(huv)=B_x, \tag{2}$$

$$\frac{\partial (hv)}{\partial t}+\frac{\partial}{\partial x}(huv)+\frac{\partial}{\partial y}\left(hv^2+\frac{1}{2}gh^2\right)=B_y, \tag{3}$$

$$\frac{\partial (hc)}{\partial t}+\frac{\partial (hcu)}{\partial x}+\frac{\partial (hcv)}{\partial y}=E-D, \tag{4}$$

$$\frac{\partial z}{\partial t}=\frac{D-E}{1-\phi}, \tag{5}$$

where B_x and B_y are source/sink terms defined as

$$B_x=-gh\frac{\partial z}{\partial x}-ghS_{fx}+\varepsilon\left(\frac{\partial^2 hu}{\partial x^2}+\frac{\partial^2 hu}{\partial y^2}\right)-\frac{(\rho_s-\rho_w)gh^2}{2\rho}\frac{\partial c}{\partial x}-\frac{(\rho_0-\rho)(E-D)u}{\rho(1-\phi)}, \tag{6}$$

$$B_y=-gh\frac{\partial z}{\partial y}-ghS_{fy}+\varepsilon\left(\frac{\partial^2 hv}{\partial x^2}+\frac{\partial^2 hv}{\partial y^2}\right)-\frac{(\rho_s-\rho_w)gh^2}{2\rho}\frac{\partial c}{\partial y}-\frac{(\rho_0-\rho)(E-D)v}{\rho(1-\phi)}. \tag{7}$$

t is the time, x and y are horizontal coordinates, h is the flow depth, u, v are depth-averaged velocities in the x-, y-directions, respectively, z is the bed elevation, c is the flux-averaged volumetric sediment concentration, g is the gravitational acceleration, S_{fx} and S_{fy} are friction slopes in the x and y directions, respectively, ε is the coefficient of turbulent viscosity or eddy coefficient, ϕ is the bed sediment porosity, E and D are substrate entrainment and deposition fluxes across the bottom boundary of flow (representing sediment exchange between the water column and bed), $\rho=\rho_w(1-c)+\rho_s c$ is the density of the water–sediment mixture, $\rho_0=\rho_w\phi+\rho_s(1-\phi)$ is the density of the saturated bed, α is the rainfall rate in excess of runoff and ρ_w, ρ_s are the densities of water and sediment, respectively. Similar equations have been presented in one-dimensional form recently by Fagherazzi and Sun (2003) and Cao et al. (2004).

Eq. (1) represents mass conservation for the water–sediment mixture. This equation differs from the traditional conservation equation for clear-water flows because of mass exchange between the flow and the erodible bed (i.e., the term involving E and D). As noted by Cao et al. (2004) this term is significant, not only in highly energetic flows encountered, for example during dam breaks, but also in fluvial systems. Eqs. (2) and (3) are equations for momentum conservation in the x- and y-directions, respectively. The terms on the left-hand side of these equations account for inertia and pressure effects in the flowing fluid. The kinematic wave equation and the normal flow condition (as discussed by Izumi and Parker, 1995) can be

recovered from the shallow water equations by neglecting these terms. The terms of the right-hand side of the momentum equations (i.e., B_x and B_y) account for sources or sinks in momentum related to (moving from left to right) bed topography, friction loss, diffusive turbulent momentum transfer associated with Reynolds' stresses, spatial variations in sediment concentration and momentum transfer due to sediment exchange between the flow and the erodible bed. These two later terms are only significant during the transport of highly concentrated flows, and thus do not appear in the classical clear-water equations. In this work (see also Garcia and Kahawita, 1986; Fiedler and Ramirez, 2000) the dependence of the turbulent viscosity ε on velocity and depth are neglected. Eq. (4) represents sediment mass conservation. Note that suspended and bed loads are not explicitly distinguished but are treated as a single mode, an approached followed by Cao et al. (2004). This assumption reflects the fact that sediment transport takes place in a continuum between pure suspended load and pure bed load. Note also that although dispersive sediment transport has been neglected this could easily be included by adding diffusion terms (e.g., see Wu, 2004). Eq. (5) links the local variation in bed elevation to sediment removed or accumulated on the bottom.

In order to close the governing equations it is necessary to specify additional relations for the friction slope and the substrate exchange fluxes across the lower flow boundary. For the friction slope, several classical equations exist, the suitability of which depend on the flow conditions. When flow is laminar as is often the case in overland flow, the Darcy–Weisbach equation is usually considered a reasonable approximation:

$$S_{fx} = \frac{fu\sqrt{u^2+v^2}}{8gh}, \quad S_{fy} = \frac{fv\sqrt{u^2+v^2}}{8gh}, \tag{8}$$

where f is the Darcy–Weisbach friction factor. Note that although f depends on the Reynolds number it is regarded as a constant in this work. For turbulent flow, the friction loss is usually approximated using the Manning equation

$$S_{fx} = \frac{n^2u\sqrt{u^2+v^2}}{h^{4/3}}, \quad S_{fy} = \frac{n^2v\sqrt{u^2+v^2}}{h^{4/3}}, \tag{9}$$

where n is Manning's roughness coefficient. The determination of the entrainment and deposition fluxes constitutes one of the most important and poorly constrained components of models for sediment transport and morphological evolution. A large number of empirical relations have been proposed, a review of which can be found in Cao and Carling (2002). For deposition of non-cohesive sediment, this study uses the relation

$$D = \omega(1-C_a)^m C_a, \tag{10}$$

where ω is the settling velocity of a single particle in tranquil water

$$\omega = \frac{\sqrt{(36v/d)^2 + 7.5\rho_s g d} - 36v/d}{2.8}.$$

v is the kinematic viscosity of water, d is the grain diameter, g is the gravitational acceleration, ρ_s is the sediment particle density, C_a is the near-bed volumetric sediment concentration and m is an exponent ($\sim$2). A value for C_a is computed from the relation $C_a = \alpha_c c$ where c is the depth-averaged volumetric sediment concentration and α_c is a coefficient larger than unity. In order so that the near-bed concentration does not exceed $(1-\phi)$ (where ϕ is the bed sediment porosity), the coefficient α_c is computed using $\alpha_c = \min(2, (1-\phi)/c)$ (see Cao et al., 2004). In the case of very fine grained cohesive sediments (not considered here), the deposition rate depends on a critical shear stress below which sediment particles begin to deposit (e.g., see Krone, 1962).

For entrainment of cohesive material, the following relation is used (see Izumi and Parker, 2000)

$$E = \beta\left(\frac{\sqrt{u^2+v^2}}{u_c} - 1\right)^{\gamma}, \tag{11}$$

where β is an entrainment coefficient, γ is an exponent (typically 1–2) and u_c is a threshold entrainment flow velocity, and $E = 0$ for $\sqrt{u^2+v^2} \leqslant u_c$. The entrainment flux for non-cohesive material is determined from the relation (see Cao et al., 2004)

$$E = \frac{160}{R^{0.8}}\frac{(1-\phi)}{\theta_c}\frac{d\,(\theta-\theta_c)U_\infty}{h}, \tag{12}$$

where $R = d\sqrt{sgd}/v$, $s = \rho_s/\rho_w - 1$, d is the sediment grain size, v is the kinematic viscosity of water, θ is Shield's parameter ($= u_*/(sgd)$), u_* is the friction velocity ($= \sqrt{f/8}\sqrt{u^2+v^2}$), U_∞ is the free surface velocity ($= (7\sqrt{u^2+v^2})/6$), θ_c is the critical value of Shield's parameter for the initiation of sediment motion, and $E = 0$ for $\theta \leqslant \theta_c$.

There are several advantages of the sediment transport formulation such as that presented here (see also Capart and Young, 1998; Cao et al., 2004).

First, the fluxes due to entrainment and deposition are treated independently, which makes sense since they are indeed governed by completely different physics. Thus, rather than sediment being either deposited or eroded depending on whether the sediment transport capacity is less than, or greater than, the actual sediment discharge, both processes will occur simultaneously and the evolution of bed topography will simply be governed by which flux is locally the greatest. Second, as already noted above, the sediment load is treated as a single mode, rather than consisting of individual bed load and suspended load components. This continuum approach is attractive not only in the ease of implementation in a model but it also makes sense physically because of the difficulty of distinguishing individual load components when both exist in nature. A drawback of this approach is that it implies that bed load and suspended load are controlled by the same physics, which is not always the case. For example, bed load transport is affected by bottom slope while suspended sediment load is not. Third, the model requires no assumptions concerning whether morphological evolution is supply-limited versus transport-limited because this will depend on the relative importance of the entrainment and deposition fluxes for any given flow conditions. Finally, because an attempt is made to clearly separate the governing equations from the empirical relations, the substrate exchange fluxes can readily by modified, either to incorporate new data and transport models as they become available or to study different applications.

3. Numerical model

Combining the governing equations with the empirical relations just specified leads to a system of five equations for the five unknowns, $h(x,y,t)$, $u(x,y,t)$, $v(x,y,t)$, $c(x,y,t)$ and $z(x,y,t)$. These equations are nonlinear and hyperbolic when $\varepsilon = 0$. For practical purposes, the solutions to (1)–(5) maintain a hyperbolic character even when $\varepsilon \neq 0$ because ε tends to be small. These solutions may involve sharp discontinuities or shocks which propagate within the domain. In this study we make use of a well established numerical technique that is both robust and reasonably accurate (Toro, 2001).

In the following text, two main formulations are presented. The first is fully coupled and involves unsteady flow, which is applicable to situations where the rate of bed deformation is comparable to that of flow evolution. The second involves steady flow which is a reasonable assumption when the rate of bed evolution is slow relative to the rate of flow evolution.

3.1. Unsteady flow

For the purposes of obtaining a numerical solution, system (1)–(5) can be split such that Eq. (5) is treated separately. Physically, this is justified by the fact that the evolution of the bed (i.e., Eq. (5) is solely governed by the local entrainment and deposition fluxes. This enables one to write the following equations:

$$\frac{\partial \mathbf{U}}{\partial t} + \frac{\partial \mathbf{E}}{\partial x} + \frac{\partial \mathbf{G}}{\partial y} = \mathbf{S}, \tag{13}$$

where $\mathbf{U}$ is the solution vector defined as

$$\mathbf{U} = \begin{bmatrix} h \\ hu \\ hv \\ hc \end{bmatrix}. \tag{14}$$

$\mathbf{E}$ and $\mathbf{G}$ are flux vectors defined as

$$\mathbf{E} = \begin{bmatrix} hu \\ hu^2 + \frac{1}{2}gh^2 \\ huv \\ huc \end{bmatrix}, \tag{15}$$

$$\mathbf{G} = \begin{bmatrix} hv \\ huv \\ hv^2 + \frac{1}{2}gh^2 \\ hvc \end{bmatrix} \tag{16}$$

and $\mathbf{S}$ is the source vector defined as

$$\mathbf{S} = \begin{bmatrix} \alpha + \frac{E-D}{1-\phi} \\ B_x \\ B_y \\ E - D \end{bmatrix}. \tag{17}$$

The matrices $\partial\mathbf{E}(\mathbf{U})/\partial\mathbf{U}$ and $\partial\mathbf{G}(\mathbf{U})/\partial\mathbf{U}$ each have four real eigenvalues (only three of which are distinct, e.g., $\lambda_{1,2} = u \pm \sqrt{gh}$ and $\lambda_3 = u$ for the first matrix) consistent with the fact that the system is hyperbolic.

3.1.1. Finite volume method

The technique used to solve system (13) is based on the finite volume method. Integrating (13) over an arbitrary element V_i (Fig. 1), the basic equation

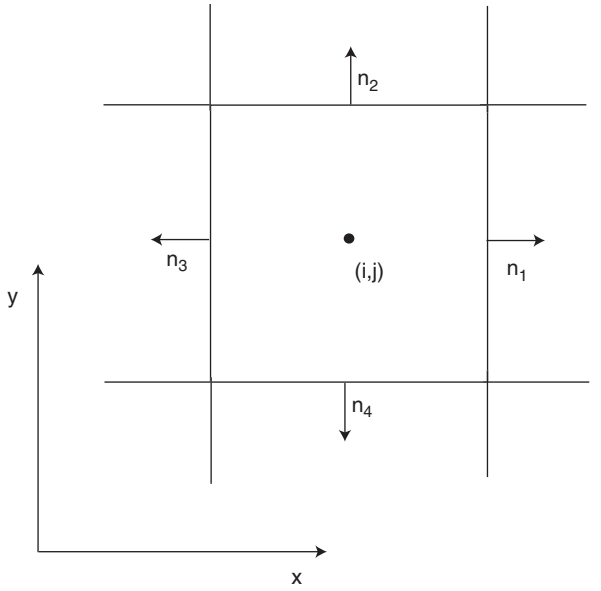

Fig. 1. Typical finite volume cell (i,j) with edges defined by four unit normal vectors.

of the finite volume method obtained using the divergence theorem is given by

$$\frac{\partial}{\partial t}\int_{V_i}\mathbf{U}\,\mathrm{d}V+\oint_{S_i}\mathbf{F}\cdot\mathbf{n}\,\mathrm{d}S=\int_{V_i}\mathbf{S}\,\mathrm{d}V, \tag{18}$$

where $\mathbf{n}$ is the outward-directed unit vector normal to boundary S_i and $\mathbf{F}$ is the flux vector. The integrand $\mathbf{F}\cdot\mathbf{n}$ is the normal flux across a surface with normal $\mathbf{n}$. Note that $\mathbf{F}\cdot\mathbf{n}$ is defined as

$$\mathbf{F}\cdot\mathbf{n}=\begin{bmatrix} h\mathbf{w}\cdot\mathbf{n} \\ hu\mathbf{w}\cdot\mathbf{n}+\frac{1}{2}gh^2n_x \\ hv\mathbf{w}\cdot\mathbf{n}+\frac{1}{2}gh^2n_y \\ hc\mathbf{w}\cdot\mathbf{n}\end{bmatrix}, \tag{19}$$

where

$$\mathbf{w}=[u\ \ v] \tag{20}$$

and

$$\mathbf{n}=\begin{bmatrix} n_x \\ n_y\end{bmatrix}. \tag{21}$$

Eq. (18) implies that the time rate of change in $\mathbf{U}$ inside a control volume depends on the total flux through the surface of the volume plus the sum of sources within the volume.

To facilitate solution of (18) we follow the approach of Zoppou and Roberts (1999) and introduce the rotation matrix $\mathbf{T_n}$,

$$\mathbf{T_n}=\begin{pmatrix} 1 & 0 & 0 & 0 \\ 0 & n_x & n_y & 0 \\ 0 & -n_y & n_x & 0 \\ 0 & 0 & 0 & 1\end{pmatrix}. \tag{22}$$

This matrix is used to align the normal $\mathbf{n}$ with the x-axis. Using the rotational invariance property of the two-dimensional shallow water equations, then

$$\mathbf{F}(\mathbf{U})\cdot\mathbf{n}=\mathbf{T_n}^{-1}\mathbf{E}(\mathbf{T_n}\mathbf{U}). \tag{23}$$

Using (23), Eq. (18) becomes

$$\frac{\partial}{\partial t}\int_{V_i}\mathbf{U}\,\mathrm{d}V+\oint_{S_i}\mathbf{T_n}^{-1}\mathbf{E}(\mathbf{T_n}\mathbf{U})\,\mathrm{d}S=\int_{V_i}\mathbf{S}\,\mathrm{d}V. \tag{24}$$

Within each control volume i the solution vector $\mathbf{U}$ is assumed to be constant. Moreover, the flux across each edge j of the control volume can be determined by the data in neighboring elements separated by edge j. Rewriting (24) in discrete form, the basic governing equation becomes

$$A_i\frac{\Delta\mathbf{U}_i}{\Delta t}+\sum_{j\in N(i)}\mathbf{T_n}^{-1}\tilde{\mathbf{E}}(\mathbf{T}_{\mathbf{n}_{i,j}}\mathbf{U}_i,\mathbf{T}_{\mathbf{n}_{i,j}}\mathbf{U}_j)L_{i,j}=A_i\mathbf{S}_i, \tag{25}$$

where $\Delta\mathbf{U}_i$ is the change in the solution vector over the time step Δt, A_i is the area of element i, $N(i)$ is the set of all elements that share an edge in common with element i, j is the index for the edges of element i, $L_{i,j}$ is the length of edge j in element i, $\mathbf{S}_i$ are the sources associated with element i, and $\tilde{\mathbf{E}}(\mathbf{T}_{\mathbf{n}_{i,j}}\mathbf{U}_i,\mathbf{T}_{\mathbf{n}_{i,j}}\mathbf{U}_j)$ is an estimate for the flux across the edge separating two neighboring elements.

3.1.2. Solution for flux

An estimate for the flux $\tilde{\mathbf{E}}(\mathbf{T}_{\mathbf{n}_{i,j}}\mathbf{U}_i,\mathbf{T}_{\mathbf{n}_{i,j}}\mathbf{U}_j)$ across the edge separating two neighboring elements in Eq. (25) can be obtained by solving a series of local Riemann problems (see Toro, 2001). The Riemann problem for a general hyperbolic system is the following initial value problem

$$\frac{\partial\mathbf{U}}{\partial t}=\frac{\partial\mathbf{E}(\mathbf{U})}{\partial x} \tag{26}$$

with initial conditions

$$\mathbf{U}(x,0)=\begin{matrix}\mathbf{U}_l, & x<0, \\ \mathbf{U}_r, & x>0,\end{matrix} \tag{27}$$

where $\mathbf{U}_l$ and $\mathbf{U}_r$ are the constant states on the left and right of any given element interface, respectively. In the formulation presented here, because the rotation matrix aligns the outward normal for

any given element edge with the x-coordinate direction, the problem involves only one-dimensional solutions oriented in the direction normal to the element interface. In this case, $\mathbf{U}_l = \mathbf{T}_{\mathbf{n}_{i,j}}\mathbf{U}_i$ and $\mathbf{U}_r = \mathbf{T}_{\mathbf{n}_{i,j}}\mathbf{U}_j$.

The structure of the Riemann problem for the two-dimensional shallow water–sediment transport equations involves three distinct waves (Fig. 2). The left and right waves (with speeds S_l and S_r, respectively) can either be shocks or rarefaction waves, whereas the middle wave (with speed S_m) is always a contact discontinuity (Toro, 2001). Contacts and shocks are discontinuous solutions whereas rarefaction waves are continuous. The region between the left and right waves is called the star region. The variables h and u are constant in the star region between the waves S_l and S_r while v and c may change discontinuously across the contact wave S_m. Because the solution for h and u is unaffected by v and c, the complete solution of the Riemann problem for the conservative quantities h and uh in the two-dimensional problem is identical to that for the one-dimensional shallow water equations.

Godunov-type methods use the solution of the Riemann problem to determine the intercell flux, which depends on the wave speeds. This study uses a first-order approximate Riemann solution based on the assumption that the left and right waves are both rarefaction waves (herein denoted HLL). With this assumption, u and h in the star region (i.e., u^* and h^*) can be determined from the initial data h_l, u_l, v_l, c_l, h_r, u_r, v_r and c_r using (Toro, 2001)

$$h^* = \frac{(u_l + 2\sqrt{gh_l} - u_r - 2\sqrt{gh_r})^2}{16g} \tag{28}$$

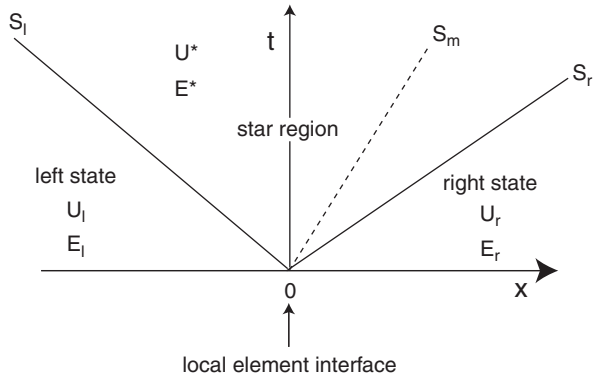

Fig. 2. Wave diagram showing structure of Riemann problem assuming a finite water depth everywhere. S_l and S_r are either shock or rarefaction waves and S_m is a contact discontinuity.

and

$$u^* = \frac{u_l + v_l}{2} + \sqrt{gh_l} - \sqrt{gh_r}, \tag{29}$$

while the wave speeds can be computed using (Toro, 1992)

$$S_l = \min(u_l - \sqrt{gh_l}, u^* - \sqrt{gh^*}), \tag{30}$$

$$S_m = u^*, \tag{31}$$

$$S_r = \max(u_r + \sqrt{gh_r}, u^* + \sqrt{gh^*}). \tag{32}$$

Using these expressions, the first two components of the inter-element flux $\tilde{\mathbf{E}}(\mathbf{T}_{\mathbf{n}_{i,j}}\mathbf{U}_i, \mathbf{T}_{\mathbf{n}_{i,j}}\mathbf{U}_j)$ can be calculated from

$$\tilde{\mathbf{E}}_{1,2}(\mathbf{U}_l, \mathbf{U}_r) = \begin{cases} \mathbf{E}_l & \text{if } S_l \geq 0, \\ \mathbf{E}^* & \text{if } S_l < 0 < S_r, \\ \mathbf{E}_r & \text{if } S_r \leq 0, \end{cases} \tag{33}$$

where

$$\mathbf{E}^* = \frac{S_r\mathbf{F}_l - S_l\mathbf{F}_r + S_lS_r(\mathbf{U}_r - \mathbf{U}_l)}{S_r - S_l}. \tag{34}$$

The third and fourth components of this flux can be determined from

$$\tilde{\mathbf{E}}_3(\mathbf{U}_l, \mathbf{U}_r) = \begin{cases} \mathbf{E}_1 v_l & \text{if } S_m \geq 0, \\ \mathbf{E}_1 v_r & \text{if } S_m < 0 \end{cases} \tag{35}$$

and

$$\tilde{\mathbf{E}}_4(\mathbf{U}_l, \mathbf{U}_r) = \begin{cases} \mathbf{E}_1 c_l & \text{if } S_m \geq 0, \\ \mathbf{E}_1 c_r & \text{if } S_m < 0, \end{cases} \tag{36}$$

where $\tilde{\mathbf{E}}_1$ is the first component of the flux calculated from (33) and $\tilde{\mathbf{E}}_{3,4}$ are the third and fourth components of $\tilde{\mathbf{E}}(\mathbf{U}_l, \mathbf{U}_r)$. Once this flux is computed for each interface of an element the local solution can be advanced to the next time step according to Eq. (25).

The wave speed estimates given by (30), (31) and (32) assume that a non-zero water depth exists everywhere. If a dry bed exists on either side of a cell interface, the eigenvalues related to S_l and S_r collapse onto one and the system of equations is no longer strictly hyperbolic. If a dry bed is to the left, the wave speeds should be computed as

$$S_l = u_r - 2\sqrt{gh_r}, \tag{37}$$

$$S_m = S_l, \tag{38}$$

$$S_r = u_r + \sqrt{gh_r}, \tag{39}$$

whereas for a dry bed on the right, the wave speeds are given by

$$S_l = u_l - \sqrt{gh_l}, \tag{40}$$

$$S_m = S_r, \tag{41}$$

$$S_r = u_l + 2\sqrt{gh_r}. \tag{42}$$

The bed is regarded as 'dry' if the water depth is less than a small value (1×10^{-6} m). Restricting the water depth from dropping below this value avoids problems when evaluating the friction terms which involve division by h (see Eqs. (8) and (9)).

3.1.3. Time stepping

Eq. (25) is solved here using the standard explicit forward Euler method. However, in order to reduce numerical instabilities associated with rapid variations in velocities and/or water depth, the friction slope terms S_{fx} and S_{fy} are evaluated point-implicitly (see Bussing and Murman, 1987; Fiedler and Ramirez, 2000). This is achieved firstly by splitting the source term in (25) into the form

$$\mathbf{S}_i = \mathbf{S}_0 + \mathbf{S}_f, \tag{43}$$

where

$$\mathbf{S}_0 = \begin{bmatrix} \alpha + \frac{E-D}{1-\phi} \\ -gh\frac{\partial z}{\partial x} + \varepsilon\left(\frac{\partial^2 hu}{\partial x^2} + \frac{\partial^2 hu}{\partial y^2}\right) - \frac{(\rho_s-\rho_w)gh^2}{2\rho}\frac{\partial c}{\partial x} - \frac{(\rho_0-\rho)(E-D)u}{\rho(1-\phi)} \\ -gh\frac{\partial z}{\partial y} + \varepsilon\left(\frac{\partial^2 hv}{\partial x^2} + \frac{\partial^2 hv}{\partial y^2}\right) - \frac{(\rho_s-\rho_w)gh^2}{2\rho}\frac{\partial c}{\partial y} - \frac{(\rho_0-\rho)(E-D)v}{\rho(1-\phi)} \\ E - D \end{bmatrix}$$

and

$$\mathbf{S}_f = \begin{bmatrix} 0 \\ -ghS_{fx} \\ -ghS_{fy} \\ 0 \end{bmatrix}.$$

All terms in $\mathbf{S}_0$ are evaluated at the previous time step, corresponding to a standard explicit scheme. For the friction terms, it is convenient to define a time-stepping coefficient β ($0 \leqslant \beta \leqslant 1$), enabling $\mathbf{S}_f$ to be written in terms of the time steps n and $n+1$ as

$$\mathbf{S}_f = (1-\beta)\mathbf{S}_f^n + \beta\mathbf{S}_f^{n+1}. \tag{44}$$

Utilizing a Taylor series expansion, the friction term can be approximated as

$$\mathbf{S}_f^{n+1} \approx \mathbf{S}_f^n + \frac{\partial \mathbf{S}_f}{\partial \mathbf{U}_i}\Delta\mathbf{U}_i, \tag{45}$$

where it should be understood that the derivatives are evaluated at the old (i.e., n) time step. Introducing (43), (44) and (45) into Eq. (25) the governing equation can be written as

$$\Delta\mathbf{U}_i = \mathbf{Q}\Delta t\left(\mathbf{S}_i - \frac{1}{A_i}\sum_{j\in N(i)} \mathbf{T}_{\mathbf{n}}^{-1}\tilde{\mathbf{E}}(\mathbf{T}_{\mathbf{n}_{i,j}}\mathbf{U}_i, \mathbf{T}_{\mathbf{n}_{i,j}}\mathbf{U}_j)\, L_{i,j}\right), \tag{46}$$

where

$$\mathbf{Q} = \left(\mathbf{I} - \Delta t\beta\frac{\partial \mathbf{S}_f}{\partial \mathbf{U}}\right)^{-1} \tag{47}$$

and $\mathbf{I}$ is the identity matrix. The advantage of this method is that the overall explicit character of the equation has been maintained but with improved stability. Nevertheless, because the scheme is explicit, the time step is constrained by the usual Courant condition. The time step is calculated from

$$\Delta t = c\ \mathrm{min}(\mathrm{d}x, \mathrm{d}y)/S_{max}, \tag{48}$$

where S_{max} is the maximum wave speed across any interface in the entire model domain and c is the Courant number which has a value in the range $0 < c \leqslant 1$.

3.1.4. Boundary conditions

Two main boundary conditions are encountered in this study: those corresponding to solid and transmissive boundaries. For a cell with a constant state $\mathbf{U} = [u\, hu\, hv\, hc]^{\mathrm{T}}$ which has an edge that forms a boundary, it is necessary to specify the unknown state $\mathbf{U}_b$ on the other side of the boundary. No flow is permitted through a solid boundary, which is implemented in this scheme by setting $\mathbf{U}_b = [u\ -hu\ hv\ hc]^{\mathrm{T}}$. A transmissive boundary is implemented by setting $\mathbf{U}_b = \mathbf{U}$.

3.2. Steady flow

In cases when the bed evolution is much slower than the rate of flow evolution, it is common practice to approximate the flow as steady while the bed is evolving (e.g., see Izumi and Parker, 1995). For this case, the system of governing equations can be written as

$$\frac{\partial(hu)}{\partial x} + \frac{\partial(hv)}{\partial y} = \alpha + \frac{E-D}{1-\phi}, \tag{49}$$

$$\frac{\partial}{\partial x}\left(hu^2 + \frac{1}{2}gh^2\right) + \frac{\partial}{\partial y}(huv) = B_x, \tag{50}$$

$$\frac{\partial}{\partial x}(huv)+\frac{\partial}{\partial y}\left(hv^2+\frac{1}{2}gh^2\right)=B_y, \tag{51}$$

$$\frac{\partial(hcu)}{\partial x}+\frac{\partial(hcv)}{\partial y}=E-D, \tag{52}$$

$$\frac{\partial z}{\partial t}=\frac{D-E}{1-\phi}, \tag{53}$$

which is identical to Eqs. (1)–(5) except that the time derivatives in (1)–(4) have been dropped. All time evolution is now related to bed evolution.

For the purpose of calculating a numerical solution to system (49)–(53) it is convenient to retain the transient terms (as in (1)–(5)) and obtain the steady-state flow solution by iteration (typically called the pseudotransient method). This approach has the advantage that the same numerical scheme used to solve the unsteady flow problem can be utilized. The general procedure involves the following steps to be performed repeatedly:

1. For a fixed topographic surface, repeatedly solve the flow problem (i.e., solve Eq. (13) using the method described in Section 3.1) until a steady-state solution is obtained, when the flow depth and/or flow velocities converge to approximately constant values.
2. Compute the entrainment and deposition fluxes and modify bed topography.
3. Recalculate flow problem described in 1.

Although the initial steady-state solution can involve a significant number of iterations, subsequent solutions typically require few iterations because one can use flow depths and velocities from the previous calculation as an initial condition (see Table 1). Thus, the method is efficient and long time scales can easily be computed.

Table 1
CPU (user) time required to complete a typical model experiment on a PC workstation with an AMD Opteron 2.0 GHz processor

Experiment	CPU time per time step (s)	Spatial resolution[a]
1D dam break	3.77×10^{-3}	3×200
1D dam break over mobile bed	0.1406	10×5000
2D dam break	0.2343	200×200
2D flow over mobile bed		
1st time step	98.7	200×200
10th time step	9.4	200×200

Note that for 2D quasi-steady flow over a mobile bed (case 4), initial time step takes an order of magnitude more time than latter steps. This is because once initial steady-state solution has been computed, it provides a more accurate initial condition for subsequent computations.

[a]Note that 1D simulations are computed with the 2D model using few elements in direction in which there is no variation.

Accurate calculation of steady-state solutions for non-homogeneous conservation laws such as Eq. (25) requires delicate balancing between flux gradients and source terms, which can prove difficult with some numerical schemes (see LeVeque, 1998). We have found no difficulty obtaining accurate solutions for the cases investigated in this study. This has been determined by comparing results computed from this model with results calculated using a second-order-accurate model based on the surface gradient method (see Zhou et al., 2001).

4. Model verification

The accuracy of the presented numerical model is assessed by comparing computed results with published solutions.

4.1. Case 1—one-dimensional dam break

The first test problem is the one-dimensional dam break over a non-erosive bed, for which there is an exact solution (Stocker, 1957). A 2000 m long horizontal, frictionless channel is investigated. Initially, a dam is located at 1000 m, separating two stagnant bodies of water with depths of 10 and 0.1 m. The dam is instantaneously removed at time = 0. This setup presents a severe test case because it involves a transition from subcritical to supercritical flow, which causes problems with some numerical schemes. To study this problem, the computational domain is subdivided into 200 segments and the Courant number c is set to a conservative value of 0.5. The solution after 50 s (Fig. 3) shows a shock wave which has propagated ~600 m downstream of the original dam, and a rarefaction wave that has propagated ~600 m upstream into the reservoir. Both waves are well resolved with the first-order approximate Riemann solver.

4.2. Case 2—two-dimensional dam break

The second test is the problem introduced by Fennema and Chaudhry (1990) which involves the instantaneous breach of a two-dimensional dam in a horizontal frictionless, non-erosive channel. There is

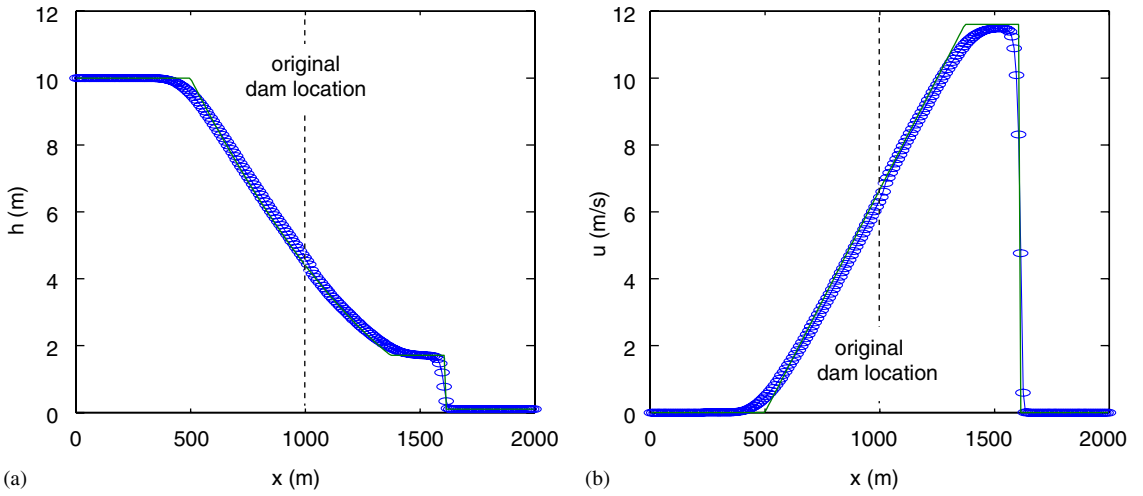

Fig. 3. Comparison between numerical solution (symbols) based on a first-order approximate Riemann solver and exact solution of Stocker (1957, solid line) after 50 s for one-dimensional dam break problem with initial water depths of 10 and 0.1 m. Error E between exact solution C_j and numerical solution c_j is 0.0176 for water depth and 0.0477 for velocity, respectively, where $E = (\sum_{j=1}^{n}|c_j - C_j|)/(\sum_{j=1}^{n}|C_j|)$ and $n = 200$. Calculation was performed in 153 time steps and required a total CPU (user) time of 0.578 s (see Table 1 for details).

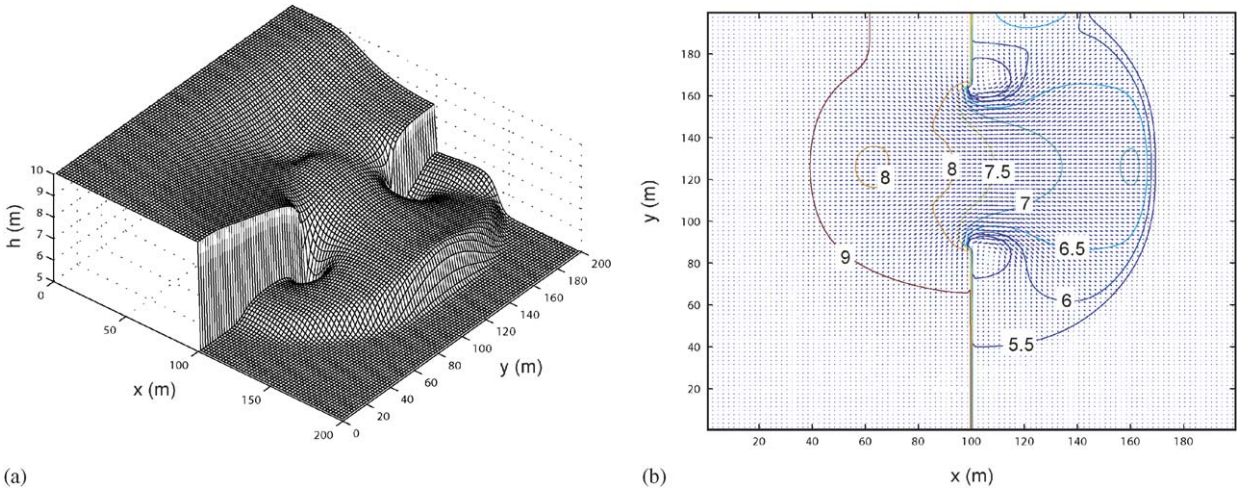

Fig. 4. Numerical solution of two-dimensional dam break problem showing water depths (a) and (b) and velocity vectors (b) after 7.2 s with initial water depths of 5 and 10 m on either side of a dam initially centered at $x = 100$ m and $y = 125$ with a 75 m wide channel. Contours in (b) are water depths in meters. Results compare well with those published in literature (e.g., see Fig. 3 of Anastasiou and Chan (1997) and Figure 11 in Mingham and Causon, 1998).

no analytical reference solution for this test case but various numerical results can be found in the literature (e.g., Fennema and Chaudhry, 1990; Mingham and Causon, 1998; Alcrudo and Garcia-Navarro, 1993; Zoppou and Roberts, 1999). A uniform cartesian mesh having 200 cells in the x-direction and 200 in the y-direction is used. A transmissive boundary is assumed at $x = 200$ m whereas the other boundaries are assumed to be solid (i.e., no flow boundaries). Two regions of initially stationary water with heights 10 and 5 m are confined to a 200 m square region by a separating wall, part of which (a 75 m wide zone centered at $y = 125$ m) is instantaneously removed at time = 0. At the instant of dam failure, water is released through a 75 m wide channel forming a bore which

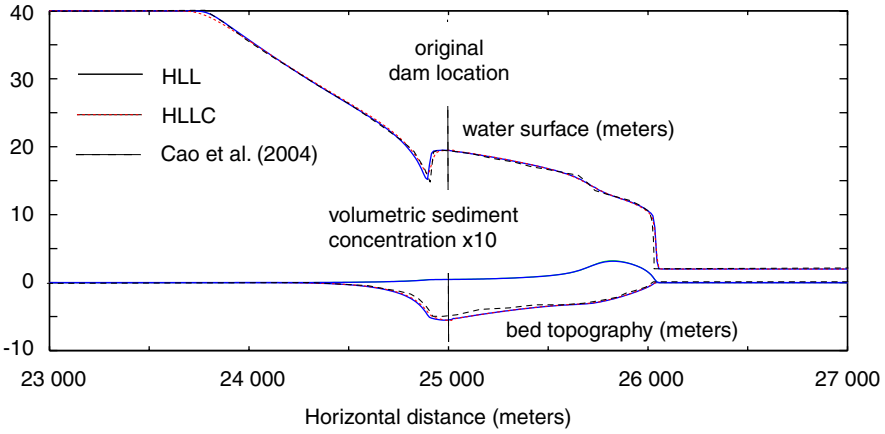

Fig. 5. Numerical solution of one-dimensional dam break over a mobile bed showing water surface, bed topography and volumetric sediment concentration (×10) after 60 s. Note good agreement between results computed with first-order numerical scheme described in this paper (solid curve labelled HLL) and a more accurate second-order total-variation-diminishing weighted average flux method used in conjunction with HLLC Riemann solver and a SUPERBEE limiter (see Toro et al., 1994), also computed here (dashed curve labelled HLLC). Results also agree well with numerical solution computed by Cao et al. (2004) (dashed curve, see their Fig. 2d, $d = 8$ mm).

propagates laterally (Fig. 4). At the same time, a negative depression wave spreads upstream into the reservoir. Computed water depths after 7.2 s compare well with results of Fennema and Chaudhry (1990) and with others (e.g., Alcrudo and Garcia-Navarro, 1993; Anastasiou and Chan, 1997; Mingham and Causon, 1998; Zoppou and Roberts, 1999).

4.3. Case 3—one-dimensional dam break over mobile bed

To test the ability to accurately calculate flow dynamics for the case of a mobile bed, numerical solutions are compared with calculations made recently by Cao et al. (2004). The model setup consists of a 50 km long, initially horizontal, one-dimensional frictional channel with a dam located at 25 km separating two initially stagnant bodies of water with depths of 40 and 2 m. The problem is discretized with 5000 cells and results are presented after 60 s. All parameters used for calculations are exactly the same as those used by Cao et al. (2004). As shown in Fig. 5, results show the development of a heavily concentrated, eroding wave front which forms at the dam and which diminishes as it propagates downstream. A hydraulic jump is formed near the dam site due to rapid bed erosion, which reaches ~5 m. This feature attenuates progressively as it propagates upstream and eventually disappears. As seen in Fig. 5, results calculated here agree closely with those computed by Cao et al. (2004).

5. Further applications

In order to demonstrate additional applications of the model we present briefly two more examples of calculations. The first illustrates the usefulness of the model for studying problems involving overland flow generated by rainfall, and in particular, for investigating channel initiation and development. This is also the first example where the steady fluid flow formulation is utilized (see Section 3.2). In this example, a 10 by 10 m initially planar surface (containing a random perturbation with a maximum amplitude of 0.01 m) with a slope of 0.2 is subjected to uniform rainfall with a rate of 10 mm/h. Substrate erosion is assumed to be governed by the cohesive law in Eq. (11) (with $\beta = 2.78\times 10^{-8}\,\mathrm{m\,s^{-1}}$, $\gamma = 1$, $u_c = 0.1\,\mathrm{m\,s^{-1}}$) whereas deposition is neglected. Bed friction is assumed to be given by the Darcy–Weisbach relation (i.e., (8)) with a constant friction factor f of 0.1. A constant eddy viscosity of 0.006 is used. Boundary conditions for the fluid are no-flow, except at the lower boundary (i.e., $y = 10$) where a transmissive boundary is assumed. Calculations are performed on a grid consisting of 200 cells in each direction. A relatively low Courant number ($c = 0.05$) is used in order to avoid numerical instabilities associated with rapid spatial variations in flow depth and velocity. Results show that

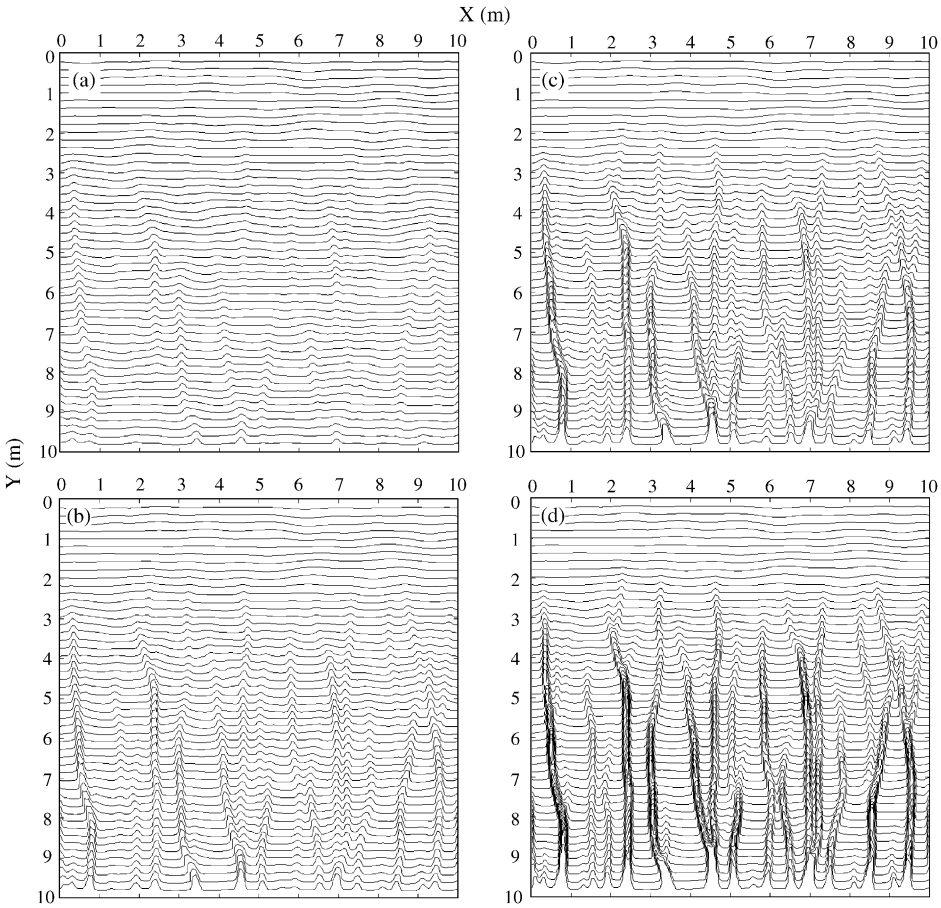

Fig. 6. Rill development on an initially planar surface subjected to uniform rainfall. Different panels show contours on topographic surface after 77.1 (a), 120.5 (b), 144.0 (c) and 190.4 (d) hours, respectively. Typical depth of rills near base of slope in final panel is ~0.2 m.

erosion in response to uniform rainfall is characterized by the formation of quasi-periodic rills which have a spacing in this case of approximately 1 m (Fig. 6). Rills begin to form ca. 2–3 m downstream of the drainage divide which is the distance required to attain the threshold flow velocity. Once initiated, rills incise and extend in a downstream direction to form a well developed network. We are currently using this model to investigate controls on channel spacing. As mentioned in the Introduction (and as discussed in detail by Izumi and Parker, 1995), this problem cannot be addressed with more simplified flow models based on normal flow (i.e., pure balance between downstream gravitational forces and resisting bed friction forces) because neglecting dynamic terms in the governing equations leads to unbound flow convergence and no finite channel spacing.

The final application considered involves computing the morphological changes associated with the impact of a train of large waves or tsunami with a coast line. The initial setup for this problem consists of a planar surface with a slope of 0.004 and a coastline located at $x = 0$ m. The water surface height at the left hand boundary is defined as a sinusoidal wave train with an amplitude of 5 m and a period of 30 min. Substrate erosion is assumed to be governed by the non-cohesive law defined in Eq. (12), deposition is described by (10) and bed friction is computed with Manning's relation ((9), all parameter values are described in the figure caption). Calculations were performed with a Courant number c of 0.01 on a grid with 200 cells. Results presented in Fig. 7 show that large amounts of sediment are eroded following the rapid retreat of waves that have extended beyond the shoreline. This sediment is deposited further offshore

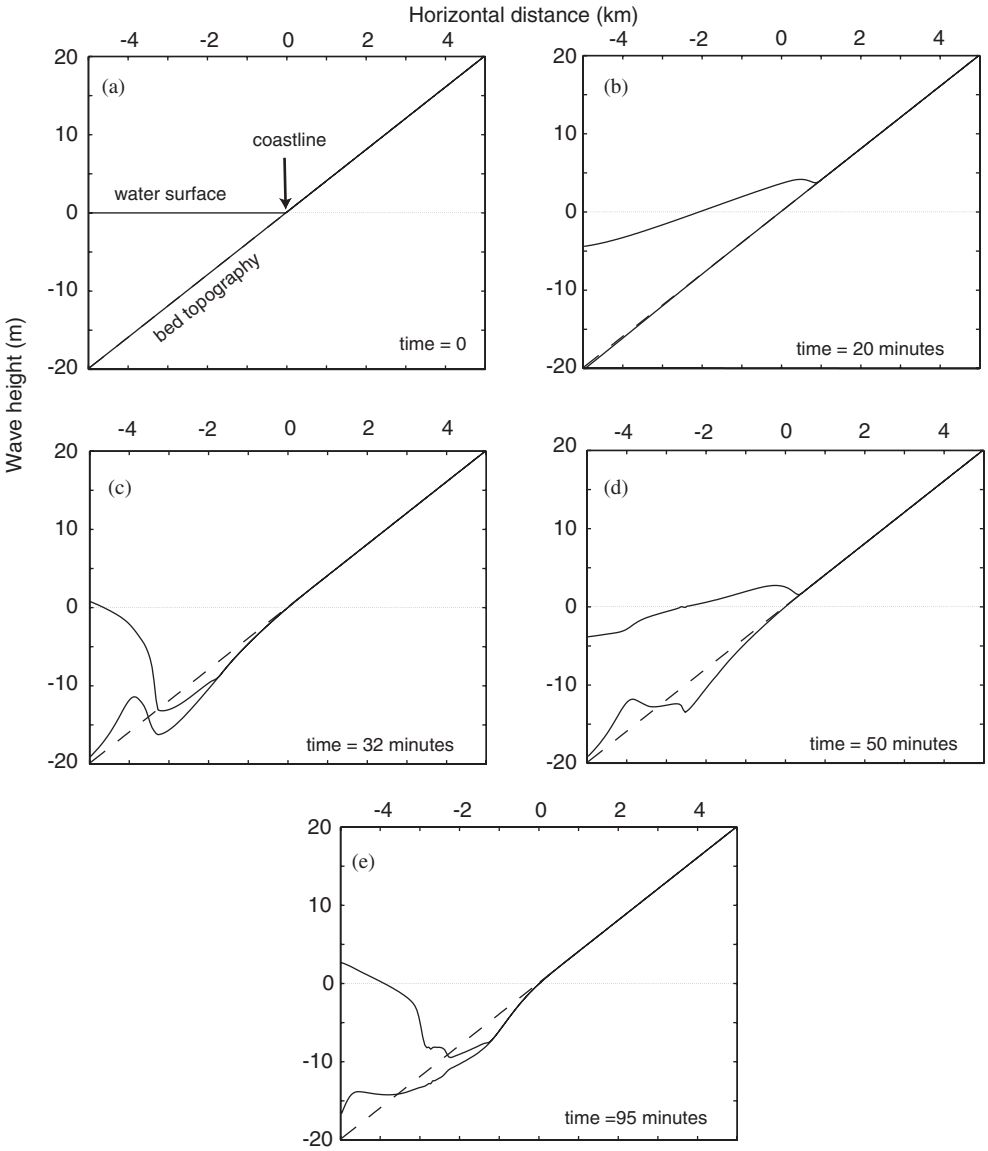

Fig. 7. Erosion and deposition induced by a train of large amplitude waves or Tsunami on a coastline. Parameters used in calculations are as follows: sediment grain size 4 mm, water density $\rho_w = 1000\,\mathrm{kg\,m^{-3}}$, solid density $\rho_s = 2600\,\mathrm{kg\,m^{-3}}$, porosity $\phi = 0.4$, deposition exponent $m = 2$, fluid viscosity $v = 1.2 \times 10^{-6}$, critical Shield's parameter $\theta_c = 0.045$, Manning's roughness coefficient $n = 0.1$.

in a large dune. The transition from erosion to deposition coincides with a large hydraulic jump. Although waves have incursions of more than 1 km inland of the original coastline, little erosion and deposition occur onshore in comparison to that observed offshore.

6. Conclusions

A model capable of simulating changes in surface morphology related to coupling between shallow water flow and sediment transport is described. The model is based on the finite volume method using a first-order approximate Riemann solver which is robust and efficient. The model produces results in very good agreement with analytical solutions as well as with published numerical results. Potential model applications include channel development related to rainfall-induced overland flow and sediment transport related to rapid events such as tsunami and/or floods.

The formulation presented in this paper offers a number of advantages over many existing models used within the Earth Science community to compute surface evolution due to flowing water. These include (1) incorporation of flow dynamics (2) non-capacity sediment transport including both supply and transport limiting cases, (3) avoidance of several poorly understood empirical relations such as drainage area–discharge, and relationships between channel width, slope, water depth, hydraulic radius and mean flow velocity. Moreover, the model presented is based on well established equations, for which robust and accurate numerical solution techniques have been developed in different fields. One purpose of this paper is to increase awareness of these existing equations and techniques within the geoscience community and thus to offer a different approach (that is consistent with research in other fields) to study problems involving coupled water flow and sediment transport.

Acknowledgments

The authors thank Alex Densmore for comments on the original manuscript and two anonymous reviewers for helpful suggestions.

References

Alcrudo, F., Garcia-Navarro, P., 1993. A high resolution Godunov-type scheme in finite volumes for the 2D shallow water equations. International Journal for Numerical Methods in Fluids 16, 489–505.

Allen, P.A., Hoffman, P.F., 2005. Extreme winds and waves in the aftermath of a Neoproterozoic glaciation. Nature 433, 123–127.

Anastasiou, K., Chan, C.T., 1997. Solution of the 2D shallow water equations using the finite volume method on unstructured triangular meshes. International Journal for Numerical Methods in Fluids 24, 1225–1245.

Bussing, T.R.A., Murman, E.M., 1987. Finite volume for the calculation of compressible chemically reacting flows. American Institute of Aeronautics and Astronautics Journal 26, 1070–1078.

Cao, Z., Carling, P.A., 2002. Mathematical modelling of alluvial rivers: reality and myth. Part I: General overview. Water Maritime Engineering 154, 207–220.

Cao, Z., Pender, G., Wallis, S., Carling, P., 2004. Computational dam-break hydraulics over erodible sediment bed. Journal of Hydraulic Engineering 130, 689–703.

Capart, H., Young, D.L., 1998. Formation of a jump by the dam break over a granular bed. Journal of Fluid Mechanics 372, 165–187.

Crave, A., Davy, P., 2001. A stochastic "precipiton" model for simulating erosion/sedimentation dynamics. Computers & Geosciences 27, 815–827.

Fagherazzi, S., Sun, T., 2003. Numerical simulations of transportational cyclic steps. Computers & Geosciences 29, 1143–1154.

Fennema, R.J., Chaudhry, M.H., 1990. Explicit methods for 2-D transient free surface flows. Journal of Hydraulic Engineering 116, 1013–1034.

Fiedler, F.R., Ramirez, J.A., 2000. A numerical method for simulating discontinuous shallow flow over an infiltrating surface. International Journal for Numerical Methods in Fluids 32, 219–240.

Garcia, R., Kahawita, R.A., 1986. Numerical solution of the St. Venant equations with MacCormack finite-difference scheme. International Journal for Numerical Methods in Fluids 6, 259–274.

Howard, A.D., 1994. A detachment-limited model of drainage basin evolution. Water Resources Research 30, 2261–2285.

Izumi, N., Parker, G., 1995. Inception of channelization and drainage basin formation: upstream-driven theory. Journal of Fluid Mechanics 283, 341–363.

Izumi, N., Parker, G., 2000. Linear stability analysis of channel inception: downstream-driven theory. Journal of Fluid Mechanics 419, 239–262.

Kooi, H., Beaumont, C., 1994. Escarpment evolution on high-elevation rifted margins; insights derived from a surface-processes model that combines diffusion, advection and reaction. Journal of Geophysical Research 99, 12191–12209.

Krone, R.B., 1962. Flume study of the transport of sediment in estuarial processes. Final Report, Hydraulic Engineering Laboratory and Sanitary Engineering Research Laboratory, University of California, Berkeley, California, USA.

LeVeque, R.J., 1998. Balancing source terms and flux gradients in high resolution Godunov methods: the quasi-steady wave-propagation algorithm. Journal of Computational Physics 146, 346–365.

Loewenherz, D.S., 1991. Stability and the initiation of channelized surface drainage: a reassessment of the short wavelength limit. Journal of Geophysical Research 96, 8453–8464.

Loewenherz, D.S., 1994. Hydrodynamic description for advective sediment transport processes and rill initiation. Water Resources Research 30, 3203–3212.

Mingham, C.G., Causon, D.M., 1998. High resolution finite-volume method for shallow water flows. Journal of Hydraulic Engineering 124, 605–614.

Roth, G., Siccardi, F., Rosso, R., 1989. Hydrodynamic description of the erosional development of drainage patterns. Water Resources Research 25, 319–332.

Simpson, G.D.H., Schlunegger, F., 2003. Topographic evolution and morphology of surfaces evolving in response to coupled fluvial and hillslope sediment transport. Journal of Geophysical Research 108, 2300.

Smith, T.R., Bretherton, F.P., 1972. Stability and the conservation of mass in drainage basin evolution. Water Resources Research 8, 1506–1529.

Stark, C.P., Stark, G.J., 2001. A channelization model of landscape evolution. American Journal of Science 301, 486–512.

Stocker, J.J., 1957. Water Waves, the Mathematical Theory with Applications. Wiley Interscience, New York.

Toro, E.F., 1992. Riemann problems and the WAF method for solving the two-dimensional shallow water equations. Philosophical Transactions of the Royal Society of London A 338, 43–68.

Toro, E.F., 2001. Shock-Capturing Methods for Free-Surface Shallow Flows. Wiley, New York, 309pp.

Toro, E.F., Spruce, M., Speares, W., 1994. Restoration of the contact surface in the HLL-Riemann solver. Shock Waves 4, 25–34.

Tucker, G.E., Slingerland, R.L., 1997. Drainage basin responses to climate change. Water Resources Research 33, 2031–2047.

Wu, W., 2004. Depth-averaged two-dimensional numerical modeling of unsteady flow and nonuniform sediment transport in open channels. Journal of Hydraulic Engineering 130, 1013–1024.

Zhou, J.G., Causon, D.M., Mingham, C.G., Ingram, D.M., 2001. The surface gradient method for the treatment of source terms in the shallow water equations. Journal of Computational Physics 168, 1–25.

Zoppou, C., Roberts, S., 1999. Catastrophic collapse of water supply reservoirs in urban areas. Journal of Hydraulic Engineering 125, 686–695.